PROGRESS IN PHOTOVOLTAICS WILEY

Thermomechanical design rules for photovoltaic modules

Andreas J. Beinert[1,2] | Pascal Romer[1] | Martin Heinrich[1] | Jarir Aktaa[2] | Holger Neuhaus[1]

[1]Fraunhofer Institute for Solar Energy Systems ISE, Freiburg, Germany

[2]Institute for Applied Materials, Karlsruhe Institute of Technology (KIT), Eggenstein-Leopoldshafen, Germany

Correspondence
Andreas J. Beinert, Fraunhofer Institute for Solar Energy Systems ISE, Heidenhofstrasse 2, 79110 Freiburg, Germany.
Email: andreas.beinert@ise.fraunhofer.de

Abstract

We present a set of thermomechanical design rules to support and accelerate future (PV) module developments. The design rules are derived from a comprehensive parameter sensitivity study of different PV module layers and material properties by finite element method simulations. We develop a three dimensional finite element method (FEM) model, which models the PV module geometry in detail from busbar and ribbons up to the frame including the adhesive. The FEM simulation covers soldering, lamination, and mechanical load at various temperatures. The FEM model is validated by mechanical load tests on three 60-cell PV modules. Here, for the first time, stress within a solar cell is measured directly using stress sensors integrated in solar cells (*SenSoCells*[®]). The results show good accordance with the simulations. The parameter sensitivity study reveals that there are two critical interactions within a PV module: (1) between ribbon and solar cell and (2) between front/back cover and interconnected solar cells. Here, the encapsulant plays a crucial role in how the single layers interact with each other. Therefore, its mechanical properties are essential, and four design rules are derived regarding the encapsulant. Also four design rules concern front and back sides, and three address the solar cells. Finally, two design rules each deal with module size and frame, respectively. Altogether we derive a set of 15 thermomechanical design rules. As a rule of thumb of how well a bill of material will work from a thermomechanical point of view, we introduce the concept of specific thermal expansion stiffness $\widehat{E}_\alpha = E \cdot \alpha \cdot A_j \cdot h$ as the product of Young's modulus E, coefficient of thermal expansion α, joint area A_j, and materials height h. The difference between two materials is a measure of how much thermal strain one material can induce in another. A strong difference means that the material with the larger value will induce thermal strain in the other.

KEYWORDS
design rules, digital prototyping, FEM simulation, PV modules, stress

1 | INTRODUCTION

Stress in solar cells plays a crucial role in the reliability of photovoltaic (PV) modules. Influences on stress are as diverse as the number of different materials in a PV module and become more and more complex with growing variety of PV modules for different applications. Nevertheless, the bill of materials development for new PV modules is often a try and error, which is very time and cost consuming. The finite element method (FEM) in combination with material characterization offers an approach for digital prototyping, which has the potential to reduce the amount of needed physical prototypes significantly. Accordingly, FEM simulations are frequently used in research as the review from Nivelle et al.[1] shows. The influence of PV modules materials was investigated sytematically by Hartley et al.,[2] who identified the glass thickness and elastic modulus as well as the material properties of used polymers as crucial parameters. The aim of this work, which is conducted within a dissertation,[3] is to derive general thermomechanical design rules for PV modules on the base of a parameter sensitivity study performed with a detailed 3D FEM model of a 60-cell PV module, including ribbons and frame. Additionally, a factor for the quick and straight forward thermomechanical assessment of materials, called specific thermal expansion stiffness $\widehat{E}_\alpha$, is introduced in Section 2. In Section 3 the FEM model is described along with its validation using solar cell integrated stress sensors. In the last section, the thermomechanical design rules are derived from the results of the parameter sensitivity study performed with the FEM model.

2 | SPECIFIC THERMAL EXPANSION STIFFNESS

To characterize materials according to their potential to induce thermal stress in the solar cells, Carroll et al.[4] introduced the so called thermal expansion stiffness E_α as the product of Young's modulus E and coefficient of thermal expansion α:

$$E_\alpha = E \cdot \alpha. \tag{1}$$

However, the thermal expansion stiffness does not take the materials dimension into account, which vary in the order of a magnitude within the PV module. Therefore, we propose to extend the thermal expansion stiffness by the materials volume V, which we call volumetric thermal expansion stiffness $\overline{E}_\alpha$:

$$\overline{E}_\alpha = E_\alpha \cdot V. \tag{2}$$

It is meant for a global description of the PV modules thermomechanics, for example the curvature after lamination due to different expansion of the PV module materials. Table 1 shows these properties for materials of conventional PV modules at room temperature.

According to the thermal expansion stiffness E_α, the ribbon has the highest impact on thermal stress. However, due to its small volume, this is a highly local influence occurring only around the ribbon itself.[5] This is represented by the low value of the volumetric thermal expansion stiffness $\overline{E}_\alpha$. In a more global perspective, the frontglass dominates the PV modules thermal strain with the highest volumetric thermal expansion stiffness $\overline{E}_\alpha$. Also, solar cells have a high thermal expansion stiffness E_α; however, due to their much smaller size, the impact on the global behavior is limited. Hence, according to the volumetric thermal expansion stiffness $\overline{E}_\alpha$, the backsheet is the material with the second strongest influence. EVA's extremely low thermal expansion stiffness value shows its buffering property at temperatures above its glass transition.[6,7]

As this discussion shows, thermomechanical stress within a PV module is complex. It has to be distinguished between local and global effects, due to strongly different layer dimensions. Small PV module components, as the ribbon, might have a high but only local impact. For such effects, the volumetric thermal expansion stiffness $\overline{E}_\alpha$ is not a reasonable measure. Therefore, we introduce a second factor, called specific thermal expansion stiffness $\widehat{E}_\alpha$. This is a further refinement of the volumetric thermal expansion stiffness $\overline{E}_\alpha$ considering only the common surface area A_j and materials height h instead of the total volume. It describes how much thermal force one material can exert to another material in contact:

TABLE 1 Dimensions, Young's modulus E, coefficient of thermal expansions α, product of them E_α, and volumetric thermal expansion stiffness $\overline{E}_\alpha$ taken to the dimensions of the reference PV module layers at room temperature

Layer	Material	Area A[mm^2]	Height h[mm]	Young's modulus E [GPa]	Coeff. of thermal expansion α [10^{-6} K^{-1}]	Therm. exp. stiffness E_α [kPa K^{-1}]	Vol. therm.exp. stiffness $\overline{E}_\alpha$ [Pa m^3 K^{-1}]
Frontglass	Soda-lime glass	1664 × 997	3.2	74[a]	9[a]	666	3529
Encapsulant	EVA	1664 × 997	0.45	0.0085[b]	270[8]	2.3	1.7
Solar cell	Cz-silicon	156.75 × 156.75	0.18	130[9]	2.62[10]	340	1.5
Backsheet	TPT	1664 × 997	0.35	3.5[7]	50.4[7]	176	102
Busbars	Silver	151.25 × 1.5	0.014	7[11]	10[12]	70	0.0002
Ribbon	Copper	151.25 × 1.5	0.2	70[9]	17[9]	1190	0.05

[a]Provided by manufacturer.
[b]Measured.[3]

$$\widehat{E}_\alpha = E_\alpha \cdot A_j \cdot h. \qquad (3)$$

Figure 1 illustrates the difference for a PV module glass as an example. We use the specific thermal expansion stiffness $\widehat{E}_\alpha$ to discuss stress within the solar cell and the volumetric thermal expansion stiffness $\overline{E}_\alpha$ to discuss the influence on the entire PV module.
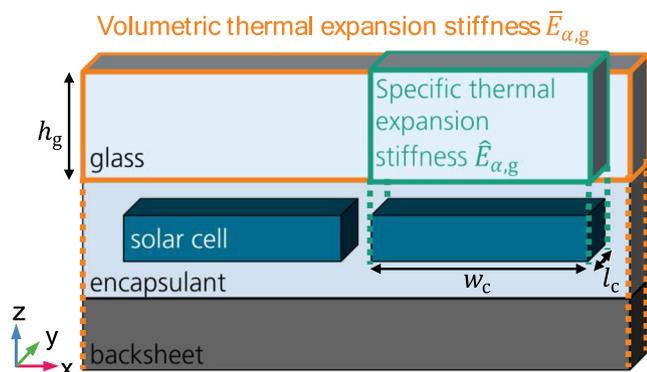

FIGURE 1 Illustration of the volume taken into account for the volumetric (orange box) and specific (green box) thermal expansion stiffness on the example of glass with regard to the solar cell, not to scale, modified after[3] [Colour figure can be viewed at wileyonlinelibrary.com]

3 | FEM MODEL

3.1 | Model

The basis of the design rules is a comprehensive parameter sensitivity study conducted with a detailed 3D FEM-model of a 60-cell PV module using COMSOL Multiphysics 5.6. Intermediate versions of this FEM-model have been published previously.[5,13,14]

To reduce the computational effort of the FEM model, we utilize the twofold axis symmetry by simulating a quarter PV module and splitting it into two components allowing for a more specific meshing, depicted in Figure 2:

1. The interconnected solar cell matrix embedded in encapsulant.
2. The front- and backsheet connected to the frame with adhesive.

For both components, we use hexahedral mesh elements with a quadratic serendipity shape function wherever applicable (component 1: 824 724 and component 2: 98 520). In component 1, the ribbons cannot be meshed by hexahedra; therefore here, we use triangular based elements (1 428 484 prisms, 8640 four-sided pyramids and 987 939 tetrahedra) and introduced a transition zone to the hexahedra, shown in Figure 2. A mesh sensitivity study is performed (not shown) to verify that the results are independent of the mesh quality.

Further assumptions and simplifications are made, like using three busbar cells with continuous busbars and neglecting front side finger
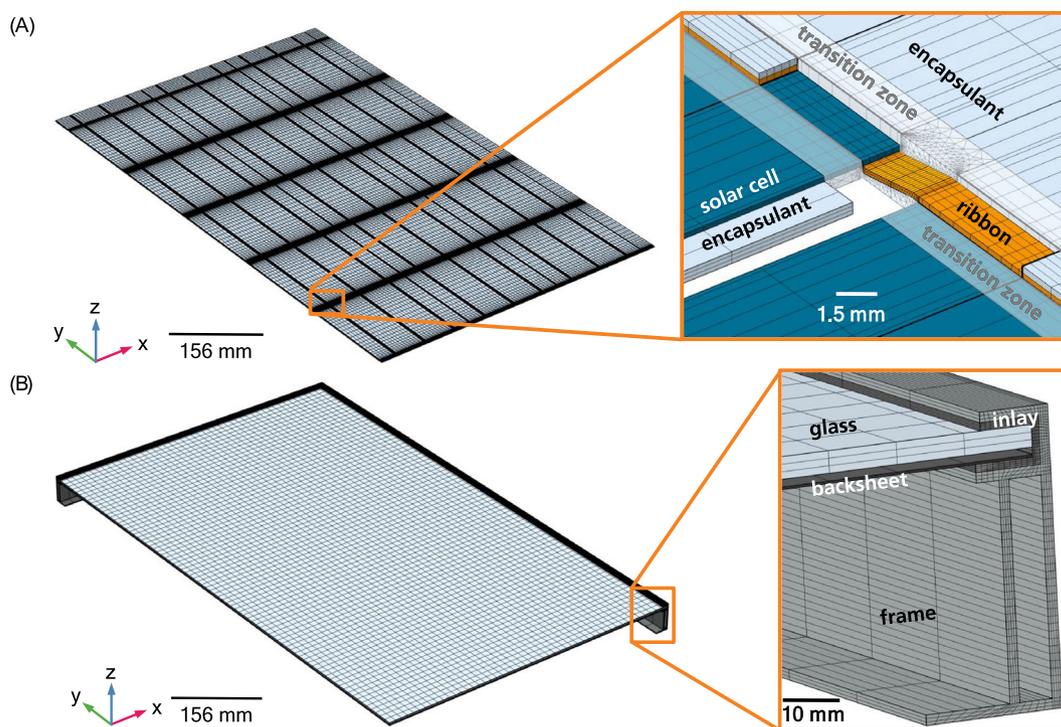

FIGURE 2 (A) Mesh of component 1 (embedded solar cell matrix). To allow a view on the solar cell and ribbon, the encapsulant (light blue) is removed partially in the insert. (B) Mesh of component 2 (frame with front- and backsheet). The insert shows a detailed view of the frame with inlay. Modified after Beinert[3] [Colour figure can be viewed at wileyonlinelibrary.com]

as well as back side aluminum metallization, using an effective material model for the ribbon by neglecting the solder layer and a simplified frame geometry. We use linear elastic temperature dependent material models published previously.[14] The cell gap as well as string gap is 3 mm. The mounting of the frame to the supporting structure is modeled by a fixed constraint at the typical contact area 20% from the frame corner on the bottom of the frame, as shown in Figure 3. A stationary geometrically linear analysis with a linear approximation for the strain (often called "smalled deformations") is used.

The FEM model covers a simplified soldering process (cooling from 179° to 25°C), lamination (cooling from 150°C to 25°C), and homogeneous surface load of 2400 Pa at different temperatures. The stress tensor from each study is transferred to the subsequent study at the temperature at which the subsequent study starts. For more details we refer to Beinert.[3]

3.2 | Validation

The soldering and lamination simulations have been validated previously.[5] Therefore, in this study, the focus is on the validation of the mechanical load simulation. For this purpose, we build three PV modules, each consisting of 58 conventional solar cells and two solar cells with integrated stress sensors (SenSoCells®)[15] positioned in the center and corner of the PV modules. A pair of sensors perpendicular to each other is positioned in the center of the solar cells, as shown in Figure 4. The senor pair is needed because the piezoresistance consists of the longitudinal and transversal effect, with the longitudinal effect being twice value of the transversal.[16] Therefore, the measured

FIGURE 4 Schematic layout of a cell with integrated piezoresistive stress sensors, not to scale, modified after Beinert.[3] At each position of the stress sensor, two sensors perpendicular to each other are implemented as indicated by the insert. Sensor pair 1 is used for the corner cell, sensor pair 2 for the center cell. [Colour figure can be viewed at wileyonlinelibrary.com]
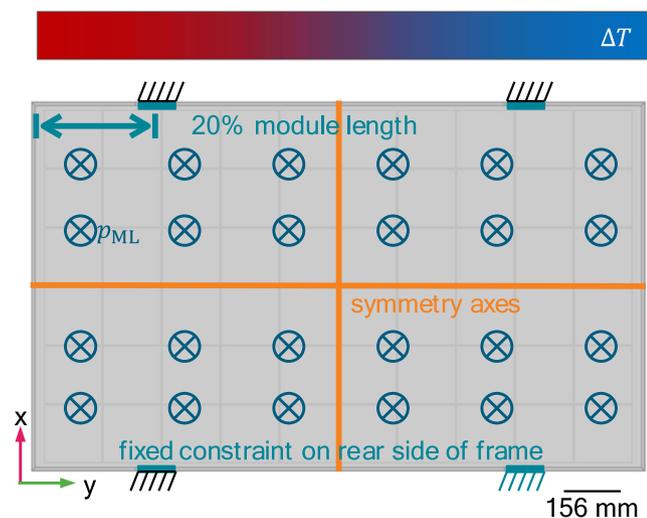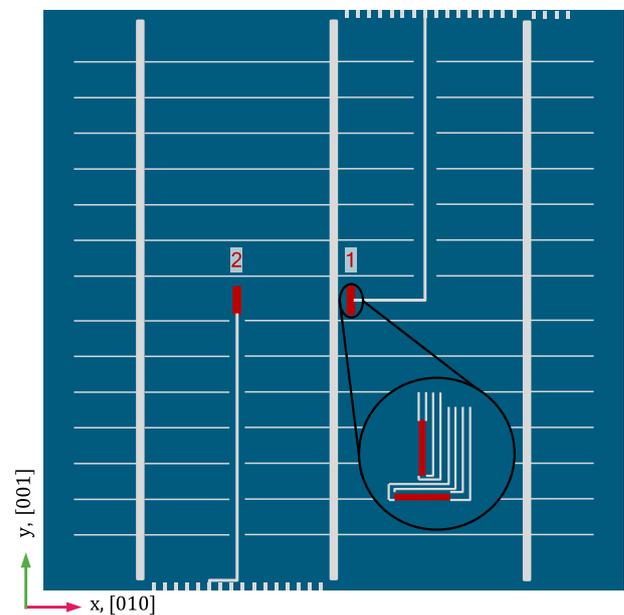

FIGURE 3 Boundary conditions used in the mechanical load study. Turquoise lines indicate the position of the fixed constraints on bottom of the frame, orange lines symmetry axes, and dark blue ⊗ constant pressure normal to the glass front side pointing towards glass surface. The color gradient from red to blue indicates different simulated temperatures. Modified after Beinert et al.[14] [Colour figure can be viewed at wileyonlinelibrary.com]

stress is a superposition of the strain in x and y; for more details, we refer to Beinert.[3] During a mechanical load test, we measure the deflection using an optical distance sensor and the stress within the solar cells using the SenSoCells®. Please note that only the stress from mechanical load is considered within the validation. We simulate the exact same setup by the FEM model. For this purpose, we use a CAD model of the actual frame instead of a simplified geometry and adapt the module layout as well as material properties.

Firstly, we analyze the PV modules deflection as a function of the applied mechanical load, depicted in Figure 5. The results show that the used linear approximation of the strain in the simulation strongly overestimates the measured deflection, although it also shows a more linear behavior. At 2400 Pa, the deviation is 28 mm (134%). Including the nonlinear strain approximation in the simulation leads to a better agreement with a deviation of 0.6 mm (2.9%).

Secondly, we analyze the stress in the center solar cells of the PV module, which is depicted in Figure 6. The stress in the FEM simulation is evaluated at the exact same position of the integrated sensor. As expected from the deflection, the linear FEM simulation strongly overestimates the measured stress by 17 MPa (76%) at 2400 Pa. Until about 1000 Pa, the geometric nonlinear FEM simulation are just slightly (<2 MPa) higher than the measurements. Above, the values diverge, which originates from a translation and torsion of the frame parts observed above 1000 Pa. The root cause is the tolerance of the frame corner connector and presumably its plastic deformation, which is explained in more detail in Beinert.[3]
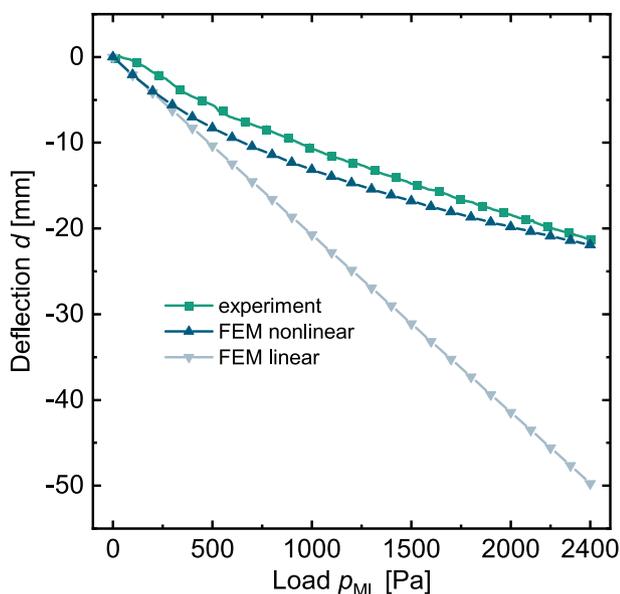
FIGURE 5 Mean measured deflection of the 3 validation modules (green square) and FEM simulation with a geometric nonlinear simulation (dark blue triangle) and linear simulation (light blue reverse triangle). Please note that the error bars of the measured deflection are too small to be visible. Modified after Beinert.[3] [Colour figure can be viewed at wileyonlinelibrary.com]
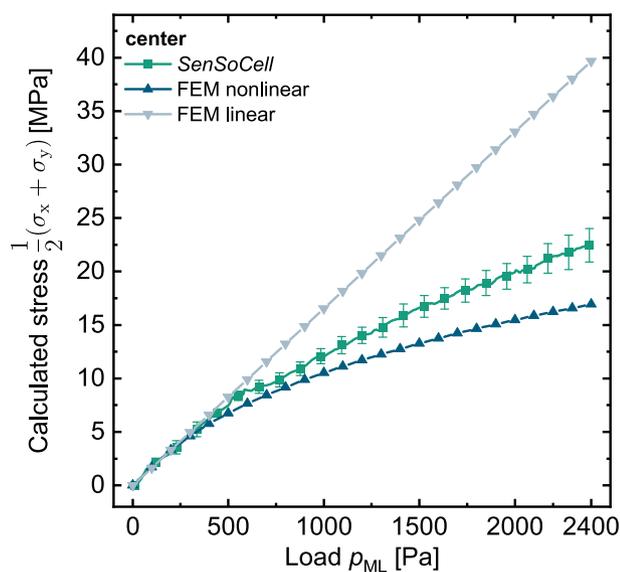

FIGURE 6 Stress calculated from resistance change of the *SenSoCell*® within the PV modules center (green square) along with the nonlinear FEM simulation (dark blue triangle) and linear FEM simulation (light blue reverse triangle). Modified after Beinert.[3] [Colour figure can be viewed at wileyonlinelibrary.com]

Thirdly, we analyze the stress in the corner *SenSoCell*, depicted in Figure 7. As opposed to the center, with −15 MPa (86%) deviation, the linear FEM simulation strongly underestimates the stress at 2400 Pa. The reason is that in the linear simulation, the direction of the applied force does not change with increasing load, which underestimates the corner displacement. Whereas in the more realistic
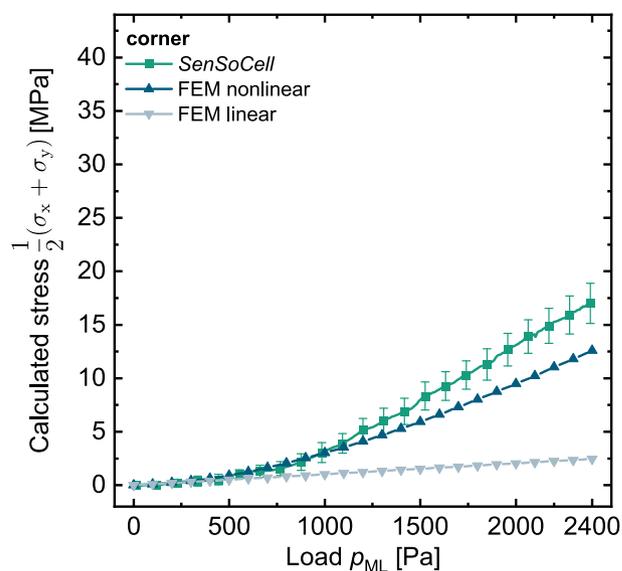

FIGURE 7 Stress calculated from resistance change of the *SenSoCell*® within the PV modules corner (green square) along with the nonlinear FEM simulation (dark blue triangle) and linear FEM simulation (light blue reverse triangle). Modified after Beinert.[3] [Colour figure can be viewed at wileyonlinelibrary.com]

geometric nonlinear simulation, the updating of the force direction with each load step leads to a more homogeneous and stronger displacement on the PV modules short edge as well as corner. Accordingly, with −5 MPa (27%) deviation, the geometric nonlinear FEM simulation is in reasonable accordance with the measured stress.

To conclude the validation experiments, we summarize the relevant findings along with their implication for the FEM model and the parameter sensitivity study.

1. The long and short parts of the used frame translate and rotate relative to each other. This results in rather linear PV module deflection as a function of applied load. While the FEM model assumes a perfect bonding of the frame parts.
2. The linear FEM simulation strongly overestimates deflection and stress in the center and underestimates stress in the corner.
3. The geometric nonlinear FEM simulation underestimates stress for higher loads.

Therefore, we conclude that the deviation between the geometric nonlinear FEM simulation and experiment originates from the differences in the frame bonding, which is specific for each frame. Since this work aims to derive general design rules, we accept the systematic deviation in favor of less computational cost.

Now, comparing the linear and geometric nonlinear FEM simulation, the results clearly show that the geometric nonlinear simulation reflects a more realistic description of the measurements. However, this comes with a huge increase in computational cost. For the validation model, the geometric nonlinear models need twice the memory (518 GB instead 262 GB) and 91 times the solution time on a faster CPU (172 h instead of 1.9 h) compared to the linear model. Therefore, the strong systematic deviation of the linear model is accepted in

favor of a broader parameter variation and hence a broader insight in the thermomechanics of PV modules. This implies that the absolute values presented are strongly overestimated, and only the relative values should be taken into consideration, which is acceptable for a comparative study.

To conclude, the geometric linear simulation overestimates the measured results, but the linear approximation is an efficient approach for a comparative identification of different influences and hence to gain a fundamental understanding of the PV module thermomechanics.

4 | THERMOMECHANICAL DESIGN RULES

The parameter sensitivity study consists of 72 parameter combinations covering the material properties shown in Table 2, different frame materials (aluminum, steel, wood), solar cell dimensions and formats as well as module sizes for glass-foil and glass–glass modules. The results of the size variation have been published previously.[14] The results are evaluated according to stress, cell fracture probability P_f, and deflection d. Due to page limitation, we refer to the authors' open access dissertation[3] for a detailed description of the used parameters as well as the simulation results. In this article, we focus on the design rules themselves.

We find two major stress causes:

1. The mismatch of thermal expansion when exposed to temperature differences.
2. The curvature of PV module and solar cells when exposed to mechanical loads.

The first one is responsible for compressive stress of solar cells after lamination as well as high tensile stress at the end of the ribbon, which dominates the cell fracture probability P_f. Both findings are in accordance with findings in the literature; for example, Eitner et al. found the stress in the solar cells after lamination and subsequent cooling to −40°C to be compressive.[7,8,17] They have not included ribbons in the FEM model, which is done by Dietrich et al.,[18] who found the largest tensile stress at the end of the ribbon. However, they do not mention how they handled the singularities occurring at the very same positions. Although measures are taken in this present work, to reduce the influence of singularities at the busbar and ribbon corners, the stress exaggeration dominates the maximum first principal stress $\sigma_{I,max}$. However, it is known that the regions around the busbar and especially at its end are prone to solar cell cracks.[19,20] Therefore, the amplitude of the stress around the busbar might not reflect the stress quantitatively correct but qualitatively it does. Consequently, the

simulated maximum first principal stress $\sigma_{I,max}$ values are overestimated and accordingly the probability of cell fracture as well. Since no other work treating singularities in PV modules were found, this has to be verified by future works.

The second one is responsible that corner solar cells show tensile stress although the deflection from mechanical load is minimal (see Figure 8). For different mounting solutions, like frameless modulus with laminate clamps, it could be shown that the highest tensile stress even occurs at the position of the largest curvature instead of the largest deflection.[13] These findings correlate to the findings of Gabor et al.[21]

For both, the material properties and dimensions play a crucial role. In the following, these influences are discussed in detail for each PV module layer, and design rules will be derived consecutively, which are also summarized in Table 3.

4.1 | Encapsulant

The encapsulant connects solar cells with the front- and backsheet, which makes it a crucial module component strongly influencing the thermomechanics. Since most of the industrial encapsulants have temperature dependent properties, in this work, two frequently used encapsulant types, EVA and TPO, with temperature dependent Young's moduli are investigated, shown in Figure 9. The values change in the order of four magnitudes within the temperature range of a PV module. Additionally, the large temperature difference of 190 K from the lamination temperature to −40°C induces high thermal stresses, which overlay with the impact of the changing Young's modulus.
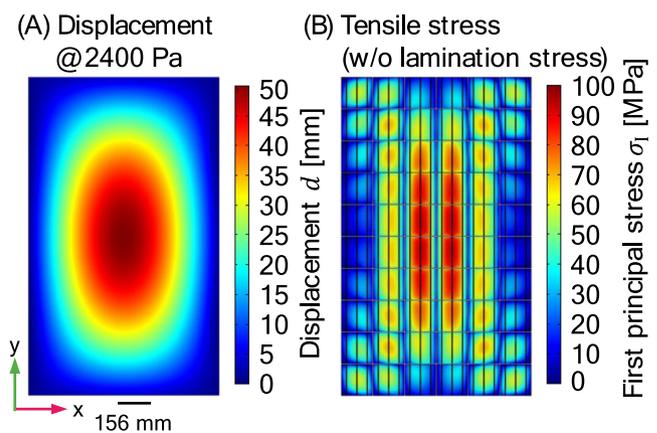

FIGURE 8 Displacement d at 2400 Pa mechanical load (A) with corresponding first principal stress σ_I in solar cells, neglecting stress after lamination (B). Modified after Beinert.[3] [Colour figure can be viewed at wileyonlinelibrary.com]

	Front/back cover	Encapsulant	Solar cells
Young's modulus E	x	x	
Coefficient of thermal expansion α	x		
Height h	x	x	x

TABLE 2 Variation of material properties of the PV module layers

TABLE 3 Summary of the derived thermomechanical design rules clustered by component. The magnitude of the influence on the stress within the solar cells is given in the last column, with increasing magnitude from $+$ to $+++$

Component	Design rule	Influence
Encapsulant	Sharp melting point with a sudden increase of the Young's modulus E_e below.	$+$
	Sharp glass transition with a sudden increase of the Young's modulus E_e.	$+$
	The encapsulants specific thermal expansion stiffness $\widehat{E}_{\alpha,e}$ should be between the ribbon $\widehat{E}_{\alpha,r}$ and solar cell $\widehat{E}_{\alpha,c}$ value: $\widehat{E}_{\alpha,r} < \widehat{E}_{\alpha,e} < \widehat{E}_{\alpha,c}$.	$++$
	Low thickness, given that there is sufficient material between ribbon and front- and backsheet and that the critical stress originates from the solar cell-ribbon interaction.	$+$
Front/back cover	At least one stiff layer is needed with a minimum thickness. For soda-lime glass around 3 mm.	$++$
	The CTE of stiff layers should have a value between the one of the solar cell and ribbon: $\alpha_c < \alpha < \alpha_r$. In symmetric module designs more critical.	$+++$
	A larger CTE of the backsheet is advantageous for push loads: $\alpha_{bs} > \alpha_{fs}$.	$+$
	For minimal bending stress: Place the solar cells in the neutral axis, e.g., by a symmetrical module design.	$++$
Solar cells	High solar cell thickness.	$++$
	Small solar cell edge length.	$+$
	Split cells: Alignment of the shorter side along the higher curvature.	$+$
PV module size	Smaller module area decreases stress.	$+$
	Module aspect ratio: longer modules instead of wider modules (for mounting on long side and non-extreme ratios).	$+$
Frame	The higher the frames stiffness, the better.	$+$
	Frame design has to be adapted to specific module design.	$+$

Accordingly, the thermomechanics at high and low temperature differ and are discussed separately below.

4.1.1 | Mechanical load above room temperature

High temperatures refer to temperatures around 85°C, the upper temperature in the thermal cycling test within the IEC 61215[22] test sequence. Around this temperature, encapsulants exhibit a low Young's modulus (see Figure 9). Therefore, the coupling of the solar cell to the front- and backsheet is relatively weak, and the coupling of the solar cell to ribbon dominates the stress within the solar cell at
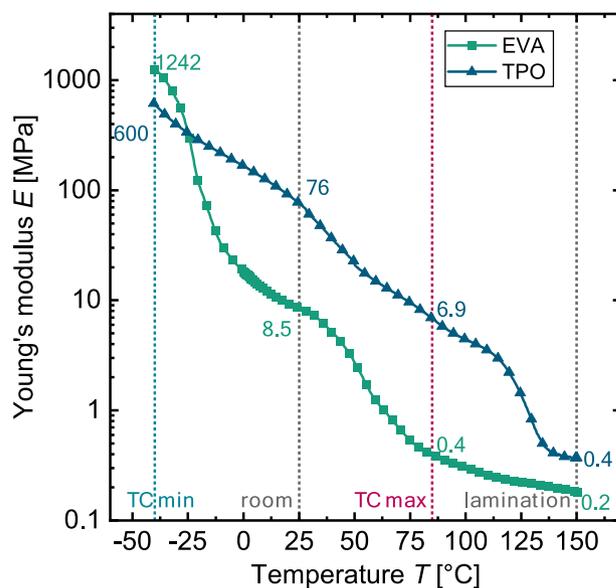

FIGURE 9 Measured temperature-dependent Young's modulus at 1 Hz of an EVA and TPO. For clarity, not all data points are shown, and the line is a guide to the eye. Modified after Beinert[3] [Colour figure can be viewed at wileyonlinelibrary.com]

mechanical load. This arises from the different contraction of ribbon and solar cell, which mainly comes from the cooling process after soldering and lamination. At lamination temperature, there is just a low stress level remaining from the soldering process. Just when the encapsulant starts to connect the solar cells to the front- and backsheet, the lamination stress starts to build up. From that moment, the maximum stress in the solar cells is a composition of solar cell-ribbon interaction and the solar cell-front-/backsheet interaction. The latter one hinders the first one depending on the strength of the coupling. For low Young's moduli, the strain absorption capacity of the encapsulant is larger, as Figure 10 shows; therefore, the coupling is lower. For higher Young's moduli, the strain absorption capacity reduces, which increases the coupling and accordingly reduces the maximum stress in the solar cells.

Therefore, at high temperatures, encapsulants with higher Young's moduli are beneficial. This could be achieved by a sharp melting point with a sudden increase of the Young's modulus below. Then again, if the Young's modulus is too large ($\widehat{E}_{\alpha,e} \approx \widehat{E}_{\alpha,c}$), the stress increases again due to the high CTE of the encapsulant in the cell-encapsulant interaction, as shown in Figure 11. So, two points, which reduce the stress in solar cells, can be concluded:

1. A sharp melting point of the encapsulant with a sudden increase of the Young's modulus E_e below it.
2. The encapsulants specific thermal expansion stiffness $\widehat{E}_{\alpha,e}$ should be between the ribbons $\widehat{E}_{\alpha,r}$ and solar cells $\widehat{E}_{\alpha,c}$ value: $\widehat{E}_{\alpha,r} < \widehat{E}_{\alpha,e} < \widehat{E}_{\alpha,c}$.

These points are an extension of the design rule by Carroll et al[4] recommending thermally soft encapsulant, that is, encapsulants with a low thermal expansion stiffness E_α.
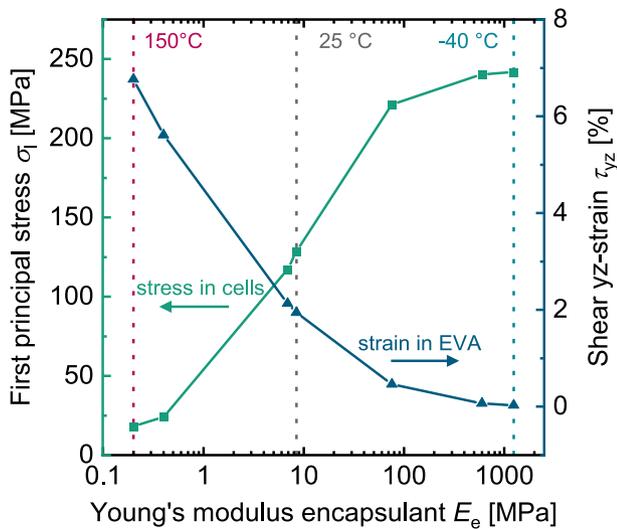
FIGURE 10 First principal stress σ_I between the busbars of the center cell (green) and the shear strain in yz-direction τ_{yz} within the EVA (blue) above the solar cell for different Young's moduli of the encapsulant at 2400 Pa mechanical load. Modified after Beinert[3] [Colour figure can be viewed at wileyonlinelibrary.com]
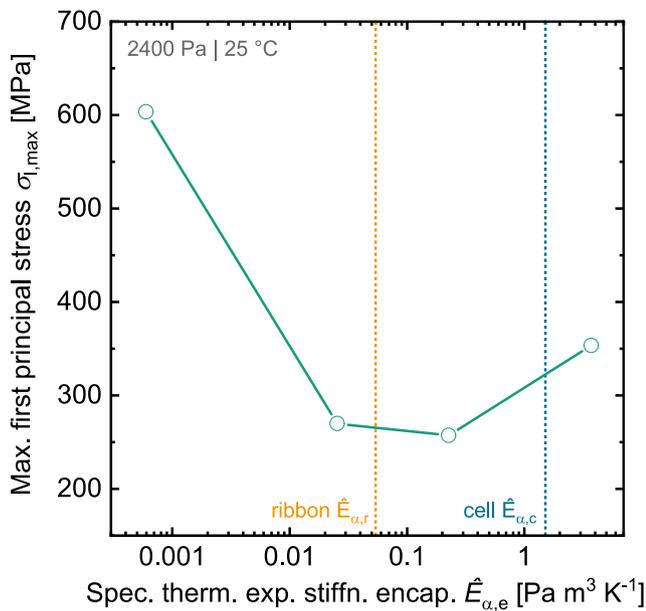

FIGURE 11 Maximum first principal stress $\sigma_{I,max}$ in solar cells at 2400 Pa push load versus the encapsulants specific thermal expansion stiffness $\hat{E}_{\alpha,e}$, and the dotted lines indicate the corresponding value of the ribbon (orange) and solar cell (blue). Modified after Beinert[3] [Colour figure can be viewed at wileyonlinelibrary.com]

4.1.2 | Mechanical load below room temperature

At room temperature, the encapsulant is in a solid state connecting the solar cells to front- and backsheet. Also, thermal stress from cooling increases due to the larger temperature difference. Accordingly, the influence of encapsulant properties increase. When reaching

lower temperatures, the thermal stress further increases. At the same time, the Young's modulus increases, reducing the deflection in mechanical load, which correlates with the experimental findings of Mühlhöfer et al.[23] They found more cracks at low temperatures, which confirms the findings of Mickiewicz et al.[24] Both conclude that the lower strain absorption of the encapsulant is responsible, which is also implied by Figure 10. However, the stress temperature dependence in Figure 12 shows that also without applied mechanical load, the maximum stress $\sigma_{I,max}$ increases, so the dominating effect is thermal stress from the solar cell–ribbon interaction. The mechanical load further increases the stress value, which is the reason why this effect is less critical in thermal cycling without mechanical load.

Another effect, which is only revealed by the FEM simulation: the stress and therefore the crack probability reduces again below $-30°C$ to values below the ones at room temperature. The reason is the steep increase of EVA's Young's modulus at the glass transition temperature (see Figure 9), which results in a lower Young's modulus until the glass transition and accordingly a higher strain absorption, that is, the solar cell-ribbon interaction dominates. In the glass transition, the coupling of the solar cells to the encapsulant and front- and backsheet increases suddenly, which reduces the maximum stress in the solar cells, as described above. This also influences the PV module bending, as the deflection at 0 Pa in Figure 12 shows. The following point can be concluded for stress reduction in solar cells:

3. A sharp glass transition of the encapsulant with a sudden increase of the Young's modulus E_e.

The encapsulants height (not shown, see Beinert[3]) has a similar impact as its Young's modulus. It defines the coupling of the solar cells to the front- and backsheet. If the coupling is too weak, the stress increases; therefore, thinner encapsulants are beneficial. However, there is a limit: when there is too little encapsulant between the ribbon and the front- and backsheet. The conclusion is:

4. Thin encapsulants reduce stress, given that there is sufficient material between ribbon and front−/backsheet.

However, this holds only if the stress from the solar cell-ribbon interaction dominates the cell fracture probability. In this work, this stress is overestimated by singularities due to rectangular busbar and ribbon shape. For lower stress overestimation, other interactions might be relevant, like the displacement of the cells and the corresponding stretching of the ribbon in the cell gap.

4.2 | Front- and backsheet

In the asymmetric glass-foil module design, the glass sheet is the dominating mechanical layer, with by far the highest specific thermal expansion stiffness $\hat{E}_{\alpha,g}$ (52 Pa m³ K⁻¹). Therefore, its properties determine the PV modules deflection in mechanical load.

FIGURE 12 Temperature influence in mechanical at 0 Pa (only temperature) (green) and 2400 Pa (blue). *Top row: left*: maximum value (open circles) and value between the busbars (filled squares) of the center cell of the first principal stress σ_I; *right*: corresponding probability of cell fracture (triangles); *bottom row: left*: third principal stress σ_{III} after lamination; *right*: deflection. Please note that the bottom ordinates depict temperature T, and the top ordinates the corresponding specific thermal expansion stiffness $\hat{E}_{\alpha,e}$. Modified after Beinert.[3] [Colour figure can be viewed at wileyonlinelibrary.com]
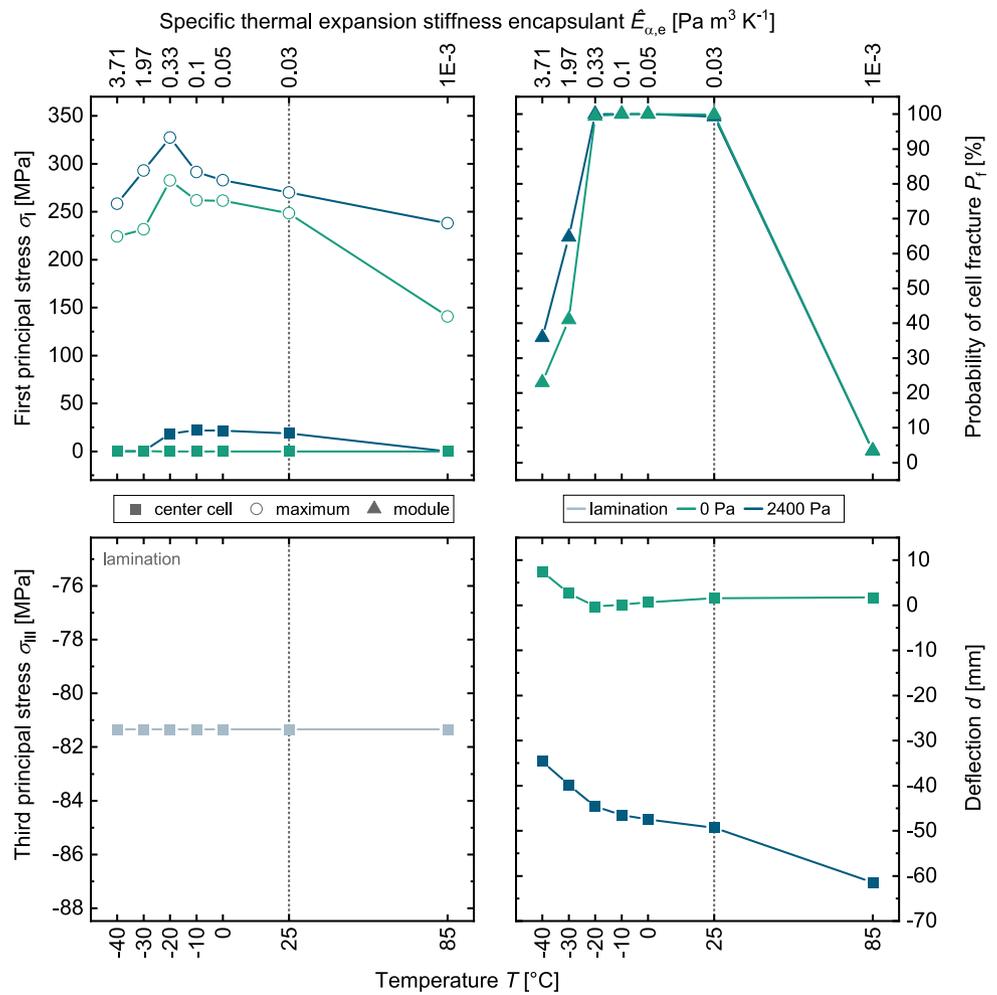
5. At least one stiff layer is needed.

In the investigated PV modules design, the optimum thickness of the soda-lime glass is around 3 mm, as shown in Beinert.[3]

The large difference of the specific thermal expansion stiffness $\hat{E}_\alpha$, to the solar cells value of 1.5 Pa m^3 K^{-1} is also the reason why the glass' height has almost no influence on thermal stress in the solar cells.

Differently, the front- and backsheet CTE strongly influences the thermal stress. For CTE values lower than the CTE of the ribbon, the thermal stress in the solar cells decreases. Much larger CTE values lead to extremely critical stresses and cell fracture probabilities. To visualize this, the relative specific thermal expansion stiffness $\hat{E}_{\alpha,rel}$ is introduced. It is the specific thermal expansion stiffness but instead of the CTE, the difference of the CTE to the ribbons value is used:

$$\hat{E}_{\alpha,rel} = E \cdot (\alpha - \alpha_r) \cdot A_j \cdot h \qquad (4)$$

Figure 13 shows the maximum first principal stress $\sigma_{I,max}$ in the solar cells versus the relative specific thermal expansion stiffness of the backsheet $\hat{E}_{\alpha,rel,bs}$ relative to the ribbons CTE ($17 \cdot 10^{-6}$ K^{-1}). The backsheet has the same impact as the frontsheet; even for glass-foil
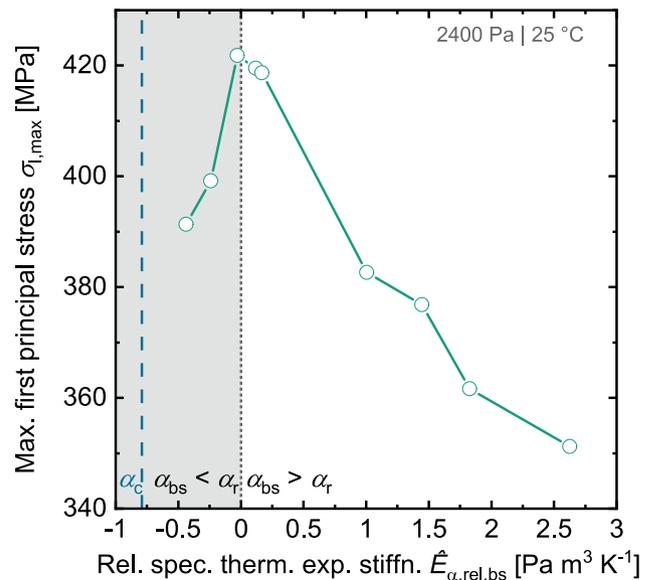

FIGURE 13 Maximum first principal stress $\sigma_{I,max}$ in solar cells at 2400 Pa push load versus the relative specific thermal expansion stiffness of the backsheet $\hat{E}_{\alpha,rel,bs}$ relative to the ribbons CTE. The dashed blue line indicates the solar cells CTE. Modified after Beinert.[3] [Colour figure can be viewed at wileyonlinelibrary.com]

modules, the impact is just smaller. This correlates to the findings of Krämer et al.[25] that the stress in solder bonds during thermal cycling is higher in glass–glass modules than in glass-foil modules. A CTE larger than the solar cell is beneficial, because the thermal compressive stress after lamination decreases the tensile stress in mechanical load:

6. The CTE of stiff layers (e.g., front- and backsheet) should have a value between the one of the solar cell and the ribbon: $\alpha_c < \alpha < \alpha_r$.

Another effect of the front and backsheet CTE is the direction of the curvature due to thermal strain. Since critical high push loads mostly occur due to a heavy accumulation of snow and ice, that is, at low temperatures, the bow from the thermal strain is opposed to the bow from the snow load and therefore reducing it. Figure 14 clearly shows the decrease of the center cell first principal stress σ_I with an increasing relative specific thermal expansion stiffness of the backsheet $\widehat{E}_{\alpha,\mathrm{rel,bs}}$ relative to the frontsheet CTE:

7. A larger CTE of the backsheet is advantageous with regard to push loads: $\alpha_{bs} > \alpha_{fs}$.

The results published by the authors previously[3,13,14,26] reflect the finding of Gabor et al.[21] that symmetric module designs, for example, glass–glass modules, are extremely robust against mechanical loads. The reason is that the solar cells are in the neutral axis. Therefore, the dominating stress is thermal stress. As mentioned above, this is larger compared to glass-foil modules. Accordingly, in symmetric designs, the material of the front- and backsheet should have a low CTE:
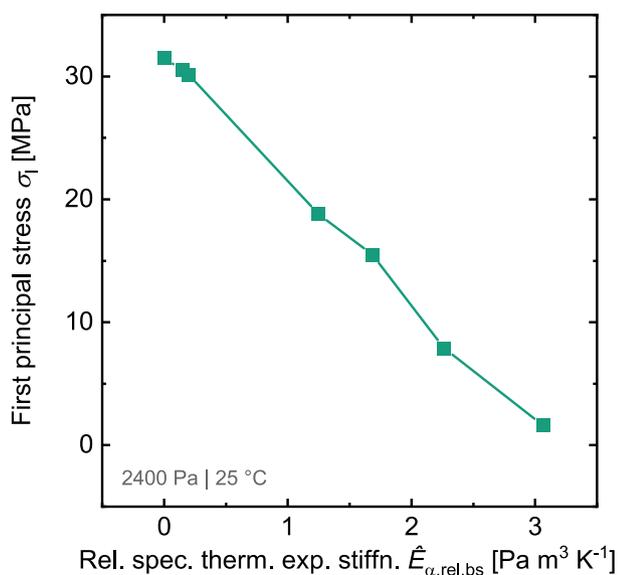

FIGURE 14 First principal stress σ_I between the busbars of the center cell at 2400 pa push load versus the relative specific thermal expansion stiffness of the backsheet $\widehat{E}_{\alpha,\mathrm{rel,bs}}$ relative to the frontsheet CTE. Modified after.[3] [Colour figure can be viewed at wileyonlinelibrary.com]

8. Minimal bending stress by placing the solar cells in the neutral axis, for example, by a symmetrical module design.

Rule 6 is in symmetric module designs more important than for asymmetric designs (glass-foil).

4.3 | Solar cell

In fact, the possibilities to reduce stress within solar cells by modifying themselves are limited to the size. The material properties are determined by its function as a semiconductor and are predominately the ones of silicon. However, the size has three different influences.

Firstly, the height. It influences the specific thermal expansion stiffness $\widehat{E}_{\alpha,c}$ and hereby the solar cells resistance to external strain. Accordingly, thicker solar cells are exposed to less stress. However, as also shown by Lai et al.,[20,27] the stress around the ribbon from soldering decreases nonlinearly with increasing cell thickness, while the compressive stress from lamination decreases almost linearly. Since the compressive stress compensates tensile stresses during mechanical load, the cell fracture probability has a minimum around 120 μm cell thicknesses. However, since this minimum strongly depends on other module materials and especially ribbons, it is different for each module design.

9. Thicker solar cells are exposed to less stress.

Secondly, the solar cell area. Increasing the solar cell area and accordingly the PV module area without adapting the frame leads to stronger deflection and accordingly higher stresses in the solar cells. Additionally, a string of small solar cells can follow the inhomogeneous frontglass curvature better than a string of large solar cells. To illustrate this, a string of solar cells is compared with a bicycle chain: A solar cell corresponds to a chain element and interconnectors in the cell gap to the flexible interconnection by pin and roller. Such as the bicycle chains with smaller elements can follow steeper socket curvatures, smaller solar cells can follow steeper frontglass curvatures. Accordingly, smaller solar cells have a smaller curvature, hence less stress, at the same frontglass curvature.

10. Smaller solar cell edge length decreases stress.

Thirdly, the size effect. The defects in solar cells are statistically distributed,[28] that is, the probability for critical defects increases with the solar cell area. Accordingly, the cell fracture probability increases with increasing overall solar cell area.

Concluding the size effects, a simple way to reduce stress and solar cell fracture probability is to split solar cells, for example into half or third cells, and align the shorter side of the solar cells along the higher curvature. To demonstrate this effect, Figure 15 compares a mechanical load FEM simulation of half-cells, which are
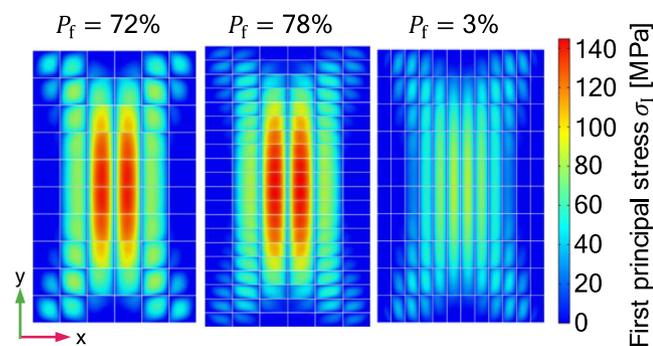
FIGURE 15 First principal stress on the back side of solar cells at 5400 Pa push load with corresponding cell fracture probability P_f with the Weibull parameters for full-cells. *Left*: full-cells; *center*: half-cells aligned along the long side of the module; *right*: half-cells aligned along the short side. Modified after Beinert.[3] [Colour figure can be viewed at wileyonlinelibrary.com]

oriented with the long edge parallel to the long PV module edge to full-cells and half-cells oriented along the short PV module edge. While the first principal stress σ_I slightly increases (due to the smaller compressive stress after lamination and larger deflection due to increasing module size), when going from full-cells to half-cells, it strongly decreases when aligning the half-cells along the short side of the PV module. Accordingly, the cell fracture probability P_f with the Weibull parameters for full-cells also strongly decreases from 78% to 3% at 5400 Pa push load. A similar behavior is observed by Podlowski et al.[29] in mechanical load tests on different PV modules with shingled solar cells. Modules with strings aligned along the short side of the PV module showed much less or no cracks compared to strings aligned along the long side. However, the cell splitting process might induce additional flaws to the splitting edge depending on the technology used.[30] Kaule et al. claim that the thermal laser separation does not influence the fracture probability; therefore, this one would be favorable.

11. Split cells: Alignment of the shorter side along the higher curvature reduces stress.

4.4 | Mounting structure and module dimension

For the rigidity of glass-foil modules, the frame is an essential module component. Its shape and dimensions have a crucial role in the deflection and curvature.[21,31,32] The results of this work show that the frames dimension and shape have to be adapted for different materials.

12. The higher the frames stiffness, the better.
13. Smaller module area decreases stress.
14. Frame design has to be adapted to specific module design.

Accordingly, it is essential to include the frame as a geometrical component in the FEM simulation rather than as boundary condition as it is a common practice in the literature.

The results also show that the PV modules aspect ratio strongly influences the deflection and hence stress in the solar cells. Assuming, that due to practical reasons, the mounting of the module takes place only along one side, long modules lead to lower stresses compared to wide modules with a similar number of solar cells, that is, power.

15. Module aspect ratio: longer modules instead of wider modules (for mounting on long side and non-extreme ratios).

5 | SUMMARY AND CONCLUSION

There are many and often entangled influences on stress within solar cells, which we summarize in the derived 15 Thermomechanical Design Rules. Additionally, we introduce three factors to characterize PV module materials easily and straightforwardly according to their influence on the thermomechanics:

1. Thermal expansion stiffness $E_\alpha = E \cdot \alpha$ as a measure of how much thermal strain a material can induce.
2. Volumetric thermal expansion stiffness $\overline{E}_\alpha = E_\alpha \cdot V$, which takes the different volume V of the PV module materials into account.
3. Specific thermal expansion stiffness $\widehat{E}_\alpha = E_\alpha \cdot A_j \cdot h$, which takes the common joining surface A_j and the height h of two joined materials into account. As a measure of how much thermal strain one material can induce in the other. For better illustration evaluating the CTE mismatch, the relative specific thermal expansion stiffness $\widehat{E}_{\alpha,rel} = E \cdot \Delta\alpha \cdot A_j \cdot h$ uses the CTE difference instead of the materials CTE.

We derive the design rules from a comprehensive parameter sensitivity study using a manifold approach: FEM simulations complemented by solar cell integrated sensors as validation. The developed FEM model covers the PV modules geometry in detail, from the busbar metallization until the frame. The analysis of the parameter sensitivity study results show that some phenomena are only revealed by this multi-scale approach.

DATA AVAILABILITY STATEMENT
The data that support the findings of this study are available from the corresponding author upon reasonable request.

ORCID

Andreas J. Beinert https://orcid.org/0000-0001-6885-3243

Pascal Romer https://orcid.org/0000-0002-2919-5572

REFERENCES

1. Nivelle P, Tsanakas JA, Poortmans J, Daenen M. Stress and strain within photovoltaic modules using the finite element method: a critical review. *Renew Sustain Energy Rev.* 2021;145:111022. doi:10.1016/j.rser.2021.111022

2. Hartley JY, Owen-Bellini M, Truman T, et al. Effects of photovoltaic module materials and design on module deformation under load. *IEEE J Photovolt.* 2020;10(3):838-843. doi:10.1109/JPHOTOV.2020.2971139

3. Beinert A. Thermomechanical design rules for the development of photovoltaic modules. Dissertation Karlsruhe; 2021.

4. Carroll W, Cuddihy E, Salama M. Material and design considerations of encapsulants for photovoltaic arrays in terrestrial applications. In: Proceedings of the 12th IEEE photovoltaic specialists conference; 1976:332-339.

5. Beinert AJ, Büchler A, Romer P, et al. Enabling the measurement of thermomechanical stress in solar cells and PV modules by confocal micro-Raman spectroscopy. *Sol Energ Mat Sol C.* 2019;193:351-360. doi:10.1016/j.solmat.2019.01.028

6. Eitner U, Kajari-Schroeder S, Koentges M, Brendel R. Non-linear mechanical properties of ethylene-vinyl acetate (EVA) and its relevance to thermomechanics of photovoltaic modules. In: Proceedings of the 25th European Photovoltaic Solar Energy Conference and Exhibition/5th World Conference on Energy Conversion; 2010:4366-4368.

7. Eitner U, Kajari-Schroeder S, Koentges M, Altenbach H. Thermal stress and strain of solar cells in photovoltaic modules. In: Altenbach H, Eremeyev VA, eds. *Shell-like Structures: Non-Classical Theories and Applications.* Berlin/Heidelberg: Springer; 2011.

8. Eitner U. Thermomechanics of photovoltaic modules. Dissertation Halle-Wittenberg; 2011.

9. Wiese S, Kraemer F, Peter E, Seib J. Mechanical problems of novel back contact solar modules. In: Proceedings of the 13th IEEE International Conference on Thermal, Mechanical and Multi-Physics Simulation and Experiments in Microelectronics and Microsystems; 2012:1-6. doi:10.1109/ESimE.2012.6191770

10. Lyon KG, Salinger GL, Swenson CA, White GK. Linear thermal expansion measurements on silicon from 6 to 340 K. *J Appl Phys.* 1977;48(3):865-868. doi:10.1063/1.323747

11. Kohn C, Faber T, Kübler R, et al. Analyses of warpage effects induced by passivation and electrode coatings in silicon solar cells. In: Proceedings of the 22nd European Photovolatic Solar Energy Conference and Exhibition (EU PVSEC); 2007:1270-1273.

12. Rendler LC, Kraft A, Ebert C, Wiese S, Eitner U. Investigation of thermomechanical stress in solar cells with multi busbar interconnection by finite element modeling. In: Proceedings of the 32nd European Photovoltaic Solar Energy Conference and Exhibition; 2016:94-98. doi:10.4229/EUPVSEC20162016-1CO.11.2

13. Beinert AJ, Ebert M, Eitner U, Aktaa J. Influence of photovoltaic module mounting systems on the thermo-mechanical stresses in solar cells by FEM modelling. In: Proceedings of the 32nd European Photovoltaic Solar Energy Conference and Exhibition; 2016:1833-1836. doi:10.4229/EUPVSEC20162016-5BV.1.14

14. Beinert AJ, Romer P, Heinrich M, Mittag M, Aktaa J, Neuhaus H. The effect of cell and module dimensions on thermomechanical stress in PV modules. *IEEE J Photovolt.* 2020;10(1):70-77. doi:10.1109/JPHOTOV.2019.2949875

15. Beinert AJ, Imm M, Benick J, et al. Silicon solar cell-integrated stress and temperature sensors for photovoltaic modules. *Prog Photovolt: Res Appl.* 2020;28(7):717-724. doi:10.1002/pip.3263

16. Smith CS. Piezoresistance effect in germanium and silicon. *Phys Ther Rev.* 1954;94(1):42-49. doi:10.1103/PhysRev.94.42

17. Eitner U, Pander M, Kajari-Schroeder S, Koentges M, Altenbach H. Thermomechanics of PV modules including the viscoelasticity of EVA. In: Proceedings of the 26th European Photovoltaic Solar Energy Conference and Exhibition; 2011:3267-3269. doi:10.4229/26thEUPVSEC2011-4EO.3.1

18. Dietrich S, Pander M, Sander M, Schulze S-H, Ebert M. Mechanical and thermo-mechanical assessment of encapsulated solar cells by finite-element-simulation. In: Proceedings of the SPIE Solar Energy and Technology; 2010. doi:10.1117/12.860661

19. Rendler LC, Romer P, Beinert AJ, et al. Thermomechanical stress in solar cells: contact pad modeling and reliability analysis. *Sol Energ Mat Sol C.* 2019;196:167-177. doi:10.1016/j.solmat.2019.03.041

20. Lai C-M, Lin K-M, Su C-H. The effects of cracks on the thermal stress induced by soldering in monocrystalline silicon cells. *Proc Institut Mech Eng Part E: J Process Mech Eng.* 2013;228(2):127-135. doi:10.1177/0954408913487285

21. Gabor AM, Janoch R, Anselmo A, Lincoln JL, Seigneur H, Honeker C. Mechanical load testing of solar panels—beyond certification testing. In: 2016 IEEE 43rd Photovoltaic Specialists Conference (PVSC); 2016-2016:3574-3579. doi:10.1109/PVSC.2016.7750338

22. International Electrotechnical Commission (IEC). *Terrestrial photovoltaic (PV) modules—design qualification and type approval—Part 2: test procedures (IEC 61215-2:2016).* Geneva, Switzerland: International Electrotechnical Commission (IEC); 2016.

23. Mülhöfer G, Berg H, Ferrara C, Grzesik W, Philipp D. Influence of mechanical load at low temperatures on cell defects and power degradation at full scale PV modules. In: Proceedings of the 28th European Photovoltaic Solar Energy Conference and Exhibition (EU PVSEC); 2013. doi:10.4229/28THEUPVSEC2013-4DO.2.2

24. Mickiewicz R, Li B, Doble D, et al. Effect of encapsulation modulus on the response of PV modules to mechanical stress. In: Proceedings of the 26th European Photovoltaic Solar Energy Conference and Exhibition; 2011:3157-3161. doi:10.4229/26thEUPVSEC2011-4CO.7.4

25. Kraemer F, Wiese S. Assessment of long term reliability of photovoltaic glass–glass modules vs. glass-back sheet modules subjected to temperature cycles by FE-analysis. *Microelectron Reliab.* 2015;55(5):716-721. doi:10.1016/j.microrel.2015.02.007

26. Beinert AJ, Leidl R, Sommeling P, Eitner U, Aktaa J. FEM-based development of novel back-contact PV modules with ultra-thin solar cells. In: *33rd European Photovoltaic Solar Energy Conference and Exhibition (EUPVSEC)*; 2017:42-47.

27. Lai C-M, Su C-H, Lin K-M. Analysis of the thermal stress and warpage induced by soldering in monocrystalline silicon cells. *Appl Therm Eng.* 2013;55(1–2):7-16. doi:10.1016/j.applthermaleng.2013.02.028

28. Möller HJ, Funke C, Rinio M, Scholz S. Multicrystalline silicon for solar cells. *Thin Solid Films.* 2005;487(1–2):179-187. doi:10.1016/j.tsf.2005.01.061

29. Podlowski L, Dörder P, Heller S, Gebrelul M, Wendlandt S. Characterization and long term stability analysis at photovoltaic modules with shingled cell strings. In: Proceedings of the 37th European Photovoltaic Solar Energy Conference and Exhibition (EU PVSEC); 2020:1027-1032. doi:10.4229/EUPVSEC20202020-4AV.1.35

30. Kaule F, Pander M, Turek M, Grimm M, Hofmueller E, Schoenfelder S. Mechanical damage of half-cell cutting technologies in solar cells and module laminates. In: SiliconPV 2018, The 8th International Conference on Crystalline Silicon Photovoltaics; 2018:20013. doi:10.1063/1.5049252

31. Schicker J, Hirschl C, Leidl R. Effect of PV module frame boundaries on stresses in solar cells. *J Energy Challenge Mech*. 2014;1(3): 155-162.

32. Tummalieh A, Beinert AJ, Reichel C, Mittag M, Neuhaus H. Holistic design improvement of the PV module frame: mechanical, optoelectrical, cost, and life cycle analysis. *Prog Photovolt: Res Appl*. 2022; 30(8):1012-1022. doi:10.1002/pip.3533